ACS OMEGA

http://pubs.acs.org/journal/acsodf

Article

ZnO Nanoparticles Modified by Carbon Quantum Dots for the Photocatalytic Removal of Synthetic Pigment Pollutants

Jing-Jing Xu, Yi-Ning Lu, Fei-Fei Tao,* Peng-Fei Liang, and Ping-An Zhang

Cite This: *ACS Omega* 2023, 8, 7845−7857

Read Online

ACCESS | Metrics & More | Article Recommendations | Supporting Information

ABSTRACT: Synthetic pigment pollutants caused by the rapid development of the modern food industry have become a serious threat to people's health and quality of life. Environmentally friendly ZnO-based photocatalytic degradation exhibits satisfactory efficiency, but some shortcomings of large band gap and rapid charge recombination reduce the removal of synthetic pigment pollutants. Here, carbon quantum dots (CQDs) with unique up-conversion luminescence were applied to decorate ZnO nanoparticles to effectively construct the CQDs/ZnO composites via a facile and efficient route. The ZnO nanoparticles with a spherical-like shape obtained from a zinc-based metal organic framework (zeolitic imidazolate framework-8, ZIF-8) were coated by uniformly dispersive quantum dots. Compared with single ZnO particles, the obtained CQDs/ZnO composites exhibit enhanced light absorption capacity, decreased photoluminescence (PL) intensity, and improved visible-light degradation for rhodamine B (RhB) with the large apparent rate constant (k_{app}). The largest k_{app} value in the CQDs/ZnO composite obtained from 75 mg of ZnO nanoparticles and 12.5 mL of the CQDs solution (~1 mg·mL^{-1}) was 2.6 times that in ZnO nanoparticles. This phenomenon may be attributed to the introduction of CQDs, leading to the narrowed band gap, an extended lifetime, and the charge separation. This work provides an economical and clean strategy to design visible-light-responsive ZnO-based photocatalysts, which is expected to be used for the removal of synthetic pigment pollutants in food industry.

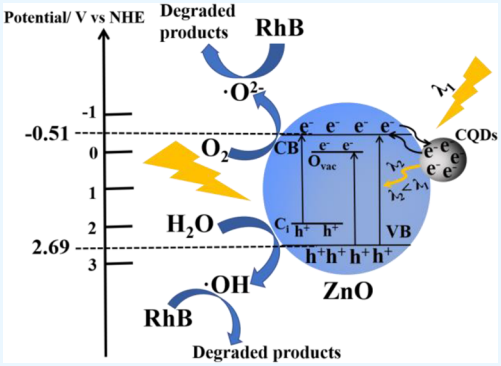

1. INTRODUCTION

As a cheap food colorant and fabric dye, rhodamine B (RhB) is commonly found in food ingredients and organic dye wastewater.[1] However, it is found that it can gradually erode ecological security and human health because of its potential genotoxicity and carcinogenicity.[2] In addition to stepping up the monitoring of the illegal use of toxic colorants, it is urgent to explore an effective, environmentally friendly, and economically practical strategy to reduce the effective concentration of toxic pollutants in biological environments, especially in water. In the past few decades, several treatment technologies for RhB removal have been established, including ion exchange,[3] membrane filtration,[4] adsorption process,[5] Fenton oxidation,[6] and photocatalytic technique.[7] In 1972, Fujishima et al. first reported the feasibility of aquatic hydrogen via a TiO_2 single crystal.[8] Subsequently, semiconductors such as TiO_2,[9] WO_3,[10] graphite carbon nitride (g-C_3N_4),[11] and ZnO[12,13] were developed as a wide variety of catalysts to decompose organic pollutants. As is well-known to all, semiconductors can absorb renewable solar radiation to produce electron and hole pairs, which contributes to the formation of active radicals including hydroxyl radicals ($^{\bullet}OH$) and superoxide radicals ($^{\bullet}O_2^-$). These active species can participate in degradation of RhB molecules.[14] Hence, photocatalysis technology is expected to become an economical and clean technique to remove synthetic pigment pollutants.[15,16]

As a widely used semiconductor material, ZnO is considered to be an attractive candidate due to its nontoxicity, unique photoelectric properties, and high catalytic activity and electron exchange performance.[17−19] However, ZnO nanostructures can only be excited under ultraviolet (UV) light due to their wide band gap of about 3.27 eV. Moreover, the fast charge recombination also can restrict its photocatalytic activity.[20−22] In order to solve the problems mentioned above, many methods have been reported for the construction of visible-light-responsive ZnO-based materials, including doping of nonmetal[23] and metal elements[24] and designing heterojunctions with semiconductors.[25] For instance, Oliveira et al. reported an effective method to synthesize a nitrogen element-doped ZnO photocatalyst for the improved photocatalytic activity of degrading RhB under UV irradiation.[26] The best efficiency of composite material significantly performed up

Received: November 28, 2022
Accepted: February 7, 2023
Published: February 16, 2023

https://doi.org/10.1021/acsomega.2c07591
ACS Omega 2023, 8, 7845−7857

to 58% more than the undoped ZnO. Andrade et al. built up the star-shaped ZnO/Ag nanostructures for the enhanced removal of methylene blue (MB) under visible-light irradiation.[27]

The modification of carbon materials can enhance the formation of photogenerated electrons and holes on semiconductors and cause the red-shift of the absorption band edge.[28] Carbon quantum dots (CQDs) with remarkable fluorescence properties have aroused widespread attention due to their up-conversion photoluminescence and excellent electron transfer ability.[29,30] The effective introduction of CQDs in ZnO can absorb more light, increase the light utilization, and facilitate the separation of charges.[31,32] Recently, there are some papers on ZnO materials decorated by CQDs for photocatalysis.[31−34] For example, Qu et al. prepared the ZnO/N,S-CQDs material for the visible-light degradation of MB.[33] Li et al. designed the ZnO/CQDs nanocomposite with the high degradation efficiency of RhB under UV light.[34] These ZnO and CQDs composites exhibit a higher photocatalytic activity under their own experimental conditions. To the best of our knowledge, there are some reports on the ZnO nanostructures modified by CQDs for the RhB degradation.[34−36] However, some composites cannot achieve the visible-light degradation of RhB, and even if it can be achieved, the degradation rate of RhB is relatively low. Therefore, this is a worthwhile work on the synthesis of the visible-light-response CQDs/ZnO composites with high degradation performance of synthetic pigment pollutant RhB.

The photocatalytic efficiency of ZnO nanomaterials can be improved through morphology optimization.[37,38] Metal−organic frameworks (MOFs) can be considered to be precursors to fabricate metallic oxide nanostructured materials via a one-step method. Metal ions act as inorganic ligand centers to bond with organic ligands, while in the process of thermal decomposition, they coalesce to increase the specific surface area and form good crystallinity nanoparticles supported by MOF fragments.[39,40] Distinctive catalytic active sites and open-framework structures derived from parent MOFs also can significantly improve the photocatalytic activity of nanophotocatalysts.[41,42] For example, ZnO nanostructures obtained by heat treatment of the zeolitic imidazolate framework-8 (ZIF-8) have more photocatalytic reactive sites and can be applied for the efficient removal of organic pollutants.[43] Payra et al. used the obtained ZnO from ZIF-8 for the photodegradation of MB, which exhibited higher catalytic activity than the ZnO nanomaterial from nitrate as precursor.[44]

Herein, using shaddock peel as the carbon source, the biomass-derived CQDs can be obtained from the facile hydrothermal synthesis. And the CQDs were embedded in ZIF-8-derived ZnO via another hydrothermal step to construct the CQD-modified ZnO composite. Based on the up-conversion luminescence of CQDs and the interface interaction of CQDs and ZnO, the composite shows enhanced visible-light photocatalytic activity and excellent stability for RhB degradation, suggesting the potential to remove synthetic pigment pollutants.

2. EXPERIMENTAL SECTION

2.1. Synthesis of the CQDs/ZnO Composites. According to the modified literature,[45] 2.5 mmol of $Zn(NO_3)_2{\cdot}6H_2O$ was added to 10 mL of deionized water under stirring for 30 min to make solution A. 25 mmol of 2-methylimidazolate was dissolved in 90 mL of deionized water by ultrasound for 30 min to obtain solution B. Then solution A was slowly added to solution B by constant stirring. After 10 min, a milk white suspension was washed by a large amount of absolute methanol 5 times and dried at 70 °C overnight to obtain ZIF-8. At last, ZIF-8 was transformed into ZnO nanoparticles by calcination in a tubular furnace at 550 °C for 4 h.

The CQD was fabricated via the modified method.[46] 25 mg of air-dried and crushed shaddock peel was placed into 40 mL of deionized water. After that, the mixture underwent the solvothermal reaction at 200 °C for 6 h. The filtered solution was dialyzed for 48 h to obtain the CQDs solution (∼1 mg·mL^{-1}).

75 mg of the prepared ZnO nanoparticles and the proper CQDs solution were evenly dispersed in the mixed solvent containing deionized water (10 mL) and absolute ethanol (6 mL). Then the mixture was heated to 140 °C for 4 h by a solvothermal method. The obtained CQDs/ZnO composites are named CZ7.5, CZ10, CZ12.5, CZ15, and CZ17.5 according to the volume of the added CQDs solution of 7.5, 10, 12.5, 15, and 17.5 mL, respectively.

2.2. Characterization. The crystal structures, morphology, and lattice fringe analysis of the samples were measured by X-ray diffraction (XRD, Empyrean XRD-6000, *Kα* radiation, λ = 0.15406 nm), scanning electron microscopy (SEM, JSM-6360 LV), and high-resolution transmission electron microscopy (HRTEM, JEM-2100F). The functional groups were studied by a Fourier transform infrared spectrometer (FT-IR, VERTEX 70) with the KBr reference. Using the Brunauer−Emmett−Teller (BET) method and the Barrett−Joyner−Halenda (BJH) model, the specific surface area and the pore size distribution were obtained by N_2 adsorption−desorption curves on a TriStar 3020. The surface composition and chemical states were conducted by X-ray photoelectron spectroscopy (XPS, ESCA Lab 250 Xi) equipped with Al Kα (1486.6 eV). The UV−visible diffusion reflection spectra (UV−vis DRS) were analyzed on a UV-2550 spectrophotometer with $BaSO_4$ as a reference. The photoluminescence (PL) curves and time-resolved photoluminescence (TRPL) spectra were taken on a fluorescence spectrometer (Fluo Time 300) with a laser of 405 nm at 293 K. The active species of $^{\bullet}O_2^-$ and $^{\bullet}OH$ were measured by electron spin resonance (ESR) spectra on a Bruker model A300 spectrometer with 5,5-dimethyl-1-pyrroline *N*-oxide (DMPO) as a trapping agent.

2.3. Photoelectrochemical Measurements. The photoelectrochemical properties were carried out on a CHI-760E electrochemical workstation (Shanghai Chenhua, China) with a 300 W Xe lamp (PLS-SXE300, Beijing Trusttech Co., Ltd.). An UV-cut optical filter was applied to obtain the visible light (λ > 420 nm). A platinum foil and an Ag/AgCl (saturated KCl) electrode were used as counter electrode and reference electrode with the electrolyte (0.5 M Na_2SO_4). The modified F-doped tin oxide (FTO) glasses as the working electrode were cleaned beforehand with acetone and absolute ethanol successively. 5 mg of catalyst was ultrasonically mixed with 1 mL of absolute ethanol. Then 0.05 mL of the as-prepared slurry was deposited on the conductive surface of the FTO glass, and the fixed active area was controlled at 0.196 cm^2. Finally, the above dried FTO glasses were heated to 300 °C for 1 h.

2.4. Photocatalytic Degradation. The photocatalytic tests were performed by the decomposition of RhB with a 300 W Xe lamp with an UV-cut optical filter (λ > 420 nm). 50 mg of sample was added to the RhB solution (50 mL, 10 mg·L^{-1}).

https://doi.org/10.1021/acsomega.2c07591
ACS Omega 2023, 8, 7845−7857

The adsorption−desorption equilibrium of photocatalysts was performed in the dark for at least 30 min before conducting the photocatalytic reaction. After a period of illumination, the reaction solution was centrifuged to obtain the supernatant. The RhB was measured on a UV−vis spectrophotometer (UV-2550) by monitoring the characteristic peak of RhB at the maximum absorption wavelength of about 553 nm. The photocatalytic degradation of other synthetic pigment pollutants (Tomato Red, Tartrazine, Apple Green, and Brilliant Blue, Shanghai Dyestuff Research Institute Co., Ltd.) was similar to that of RhB.

2.5. Trapping Experiments. To confirm the reactive groups related to the RhB degradation, the $^{\bullet}OH$, holes (h^+), and $^{\bullet}O_2^-$ can be trapped by the scavengers of *tert*-butyl alcohol (TBA), disodium ethylenediaminetetraacetate dehydrate (EDTA-2Na), and benzoquinone (BQ) with the original concentration (1 mmol·L^{-1}), respectively.[47] The experimental processes under visible light for 30 min were similar to those of the photocatalysis experiments.

Nitroblue tetrazolium (NBT) can be used as a molecular probe to monitor the generated $^{\bullet}O_2^-$ radicals during the photocatalysis. 30 mg of sample was added to NBT solution (30 mL, 0.025 mmol·L^{-1}). The optical maximum absorption peak intensity of NBT solution at 259 nm was recorded on a UV−vis spectrophotometer (UV-2550).[48] The reaction product of terephthalic acid (TA) and $^{\bullet}OH$ radicals is 2-hydroxyterephthalic acid (HTA) with a strong fluorescence emission at 425 nm.[49] In detail, 30 mg of photocatalyst was added to the TA solution (30 mL, 0.5 mmol·L^{-1} in 2 mmol·L^{-1} NaOH). The HTA from the reaction of TA and $^{\bullet}OH$ radicals was detected on the photoluminescence spectrometer (F-7000, λ_{exc} = 300 nm).

3. RESULTS AND DISCUSSION

3.1. Crystallinity and Morphology Analysis. In the XRD patterns of ZnO nanoparticles and the CQDs/ZnO composites (Figure 1), all of the characteristic diffraction peaks of ZnO nanoparticles are assigned to hexagonal wurtzite ZnO (JCPDS card no. 36-1451).[50] The CQDs/ZnO composites have XRD patterns similar to those of ZnO nanoparticles. No significant diffraction peak of CQDs in the composite is found due to the low content and/or amorphous features of CQDs.[35] The characteristic diffraction peaks of the composites are in good agreement with those of ZnO nanoparticles, indicating that the modification of CQDs hardly affects the crystallinity of ZnO nanoparticles.[51]

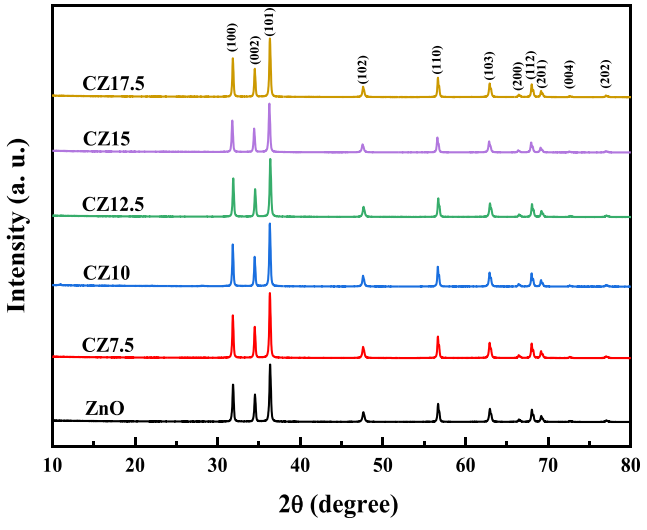

Figure 1. XRD spectra of ZnO nanoparticles and the CQDs/ZnO composites.

The SEM image of the ZnO nanoparticles is shown in Figure S1a, and a large amount of nanoparticles can be found. From the HRTEM image of Figure 2a, the synthesized ZnO is a kind of spherical nanoparticle with an average size of about 80 nm. In Figure 2b the lattice fringes of 0.28 nm are in good agreement with the (100) crystal plane of ZnO.[52] The HRTEM diagram of the CQDs shows that the CQDs with the diameter of 2−3 nm are uniformly dispersed without any aggregation (Figure 2c). The lattice fringes of d = 0.32 nm that can be obviously observed in Figure 2d correspond well to the (002) plane of CQDs.[34] Based on the SEM image of CZ12.5 (Figure S1b), the spherical nanostructures similar to ZnO nanoparticles are found with the good dispersibility and a rough surface, which may be from the modification of CQDs. According to the HRTEM investigation of CZ12.5, the CQDs are well decorated on the surface of ZnO nanoparticles (Figure 2e). The observed lattices with d = 0.28 and 0.32 nm in Figure 2f match well with the (100) crystal plane of ZnO[52] and the (002) crystal plane of CQDs,[34] which strongly proves that the CQDs are modified on the ZnO nanoparticles and the composite is composed of ZnO nanoparticles and the CQDs.

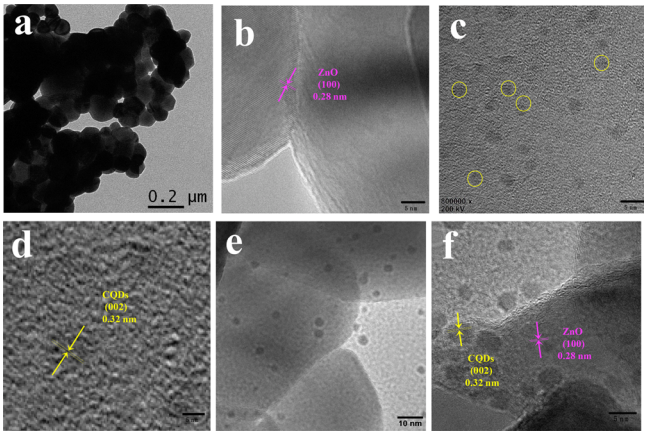

Figure 2. HRTEM images of ZnO nanoparticles (a, b), CQDs (c, d), and CZ12.5 (e, f).

It is known that ZnO nanoparticles with a spherical shape can be fabricated from the ZIF-8 precursor that has crystalline tridimensional networks consisting of Zn(II) ions bridged tetrahedrally via 2-methylimidazole ligands. Normally, ZIF-8 can decompose at above 400 °C in air and produce CO_2 and NO_x, leading to the formation of ZnO.[42] Therefore, during the calcination procedure of 550 °C in this work, the ZIF-8 crystalline structures tend to collapse and the Zn(II) ions transform into ZnO. Meanwhile, the escape of the CO_2 and NO_x gas molecules can promote the formation of nanoparticles and produce the porous structure, resulting in the generation of ZnO nanoparticles. Using the crushed shaddock peel as a precursor, the CQDs solution was obtained by the solvothermal reaction. These small fruit cells can form relatively large carbon-based fragments or CQDs under a high reaction temperature and high pressure in the autoclave.[53]

https://doi.org/10.1021/acsomega.2c07591
ACS Omega 2023, 8, 7845−7857

When the ZnO nanoparticles were mixed with the CQD solution, the CQDs/ZnO composites were synthesized by the solvothermal method. During this method, the CQDs can be coated at the surface of ZnO nanoparticles by a chemical bond through −OH groups.[54] The interface mismatch between the ZnO nanoparticles and CQDs can be minimized due to the small size of CQDs, resulting in the construction of the CQDs/ZnO composite with intimate interface contacts.[55] Furthermore, this could help to diminish the barriers for electron transport through the CQDs, which is expected to obtain the enhanced photocatalytic properties.

The ZnO nanoparticles and the CQDs/ZnO composites were analyzed to make clear the surface functional groups by FT-IR technology (Figure 3). As can be seen, for ZnO

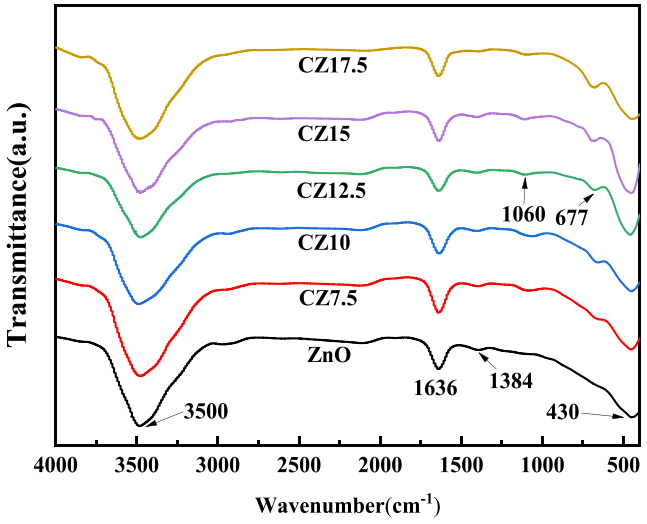

Figure 3. FT-IR spectra of ZnO nanoparticles and the CQDs/ZnO composites.

nanoparticles the peaks at 430 and 1384 cm^{-1} correspond to the Zn−O stretching vibration and the bending vibration of the bridging hydroxyl on the surface of ZnO, respectively.[56] The peak at 1636 cm^{-1} represents the O−H bending vibration, and the broad band at 3500 cm^{-1} is assigned to the stretching mode of hydroxyl groups belonging to adsorbed water molecules on the sample.[57,58] All peaks appearing in pure ZnO are also observed in the spectra of the CQDs/ZnO composites. Moreover, the absorptions at 1060 and 677 cm^{-1} correspond to the C−O−C and C═C groups, respectively.[59] The peak intensity of the C═C bond increases with the increase of CQD content, which provides further evidence for the successful introduction of CQDs.

The chemical composition of the samples was examined by using XPS analysis (Figure 4).[35,60] Based on the full survey spectra in Figure 4a, both the ZnO nanoparticles and the CQDs/ZnO composite consist of Zn and O elements, and the C peak can be found in CZ12.5, further confirming the HRTEM result. The C element detected in the ZnO nanoparticles might be attributed to adventitious hydrocarbon in the instrument. It is found in Figure 4b that the Zn 2p peaks of ZnO nanoparticles at 1020.9 and 1044.0 eV are assigned to Zn $2p_{3/2}$ and Zn $2p_{1/2}$, due to the spin orbital splitting, suggesting the existence of Zn^{2+} in the sample.[61] For pure ZnO nanoparticles in Figure 4c, the O 1s peaks at 529.8 and 532.0 eV are attributed to the lattice oxygen and surface adsorbed oxygen in O−H groups, and the peak at 531.1 eV is associated with oxygen vacancies or defects (O_{vac}).[62] The CZ12.5 shows the higher binding energy values of O 1s than ZnO nanoparticles, indicating the interface interaction of ZnO and CQDs.[63] The CZ12.5 displays the higher relative intensity of the O_{vac} peak, which shall be attributed to the addition of CQDs to cause the generation of more O_{vac} in the growth process. The surface oxygen vacancies or defects not only act as an active center to promote the adsorption but also narrow the band gap of ZnO to increase the light absorption.[62] For CZ12.5, the C 1s peaks of 284.7, 286.2, and 288.5 eV (Figure 4d) are related to the C−C bonds in adventitious carbon and sp^2-hybridized carbon from aromatic networks, the oxygen-bound species C−O and C═O groups,[63,64] implying the existence of CQDs in the composite. The small peak at 283.6 eV can be assigned to Zn−C bonds in connection with O_{vac} because of the additional electron density from negatively charged O_{vac} on the C in the Zn−C−O_{vac} bond.[63,64] Therefore, the generation of Zn−C and O_{vac} can reduce the band gap and improve the visible-light response in the CQDs/ZnO composites.[64]

In order to make clear the porous features of the CQDs/ZnO composite, the ZnO nanoparticles and CZ12.5 were characterized by the N_2 adsorption−desorption isotherms (Figure 5). Both the ZnO nanoparticles and CZ12.5 show the typical IV isotherms with a distinct hysteresis loop at a high relative pressure (P/P_0) of 0.85−1.0, further validating the existence of mesoporous structure.[16,65] The CZ12.5 has a BET-specific surface area of 7.87 $m^2 \cdot g^{-1}$ that was 1.86 times of ZnO nanoparticles. In the inset of Figure 5b, the CZ12.5 sample displays the two types of pores. One is the mesopore with a size of less than 11 nm from the own sample, and the other is the macropore with a size of about 78 nm from the disordered aggregation of nanoparticles.[18] For the ZnO nanoparticles, the pore size is mainly distributed at about 58 nm due to the aggregation of nanoparticles. Therefore, the introduction of the CQDs in the ZnO nanoparticles promotes the formation of the smaller size pores, thereby improving the specific surface area.[66]

Table 1 lists the specific surface area, pore volume, and average pore diameter of various samples. Compared with ZnO nanoparticles, the CQDs/ZnO composites have high specific surface areas that become larger with the increase of the CQD content. This may be due to the introduction of the CQDs with the small size on the ZnO nanoparticles, thereby inhibiting the accumulation of ZnO nanoparticles and enhancing the photocatalytic properties.

3.2. Optical Properties. The light absorption capacity and the separation of photogenerated charge carriers are very key factors to determine the photocatalytic performance. The UV−vis spectrum can be applied to investigate the light absorption performance. It is found in Figure 6a that the ZnO nanoparticles can only absorb light less than 400 nm, meaning that its light response range is mainly concentrated in the UV region.[18,52] Meanwhile, the CQDs/ZnO composites display continuous absorption edges in the visible region with increasing addition of CQDs. It indicates that the CQDs can broaden the light response to the visible region, thereby absorbing more photons. The CQDs can not only utilize visible light but also have up-converted luminescence.[56] Therefore, the CQDs/ZnO composites have an enhanced light absorption capacity. The excessive incorporation of CQDs will trigger the internal agglomeration of CQDs and

https://doi.org/10.1021/acsomega.2c07591
ACS Omega 2023, 8, 7845−7857

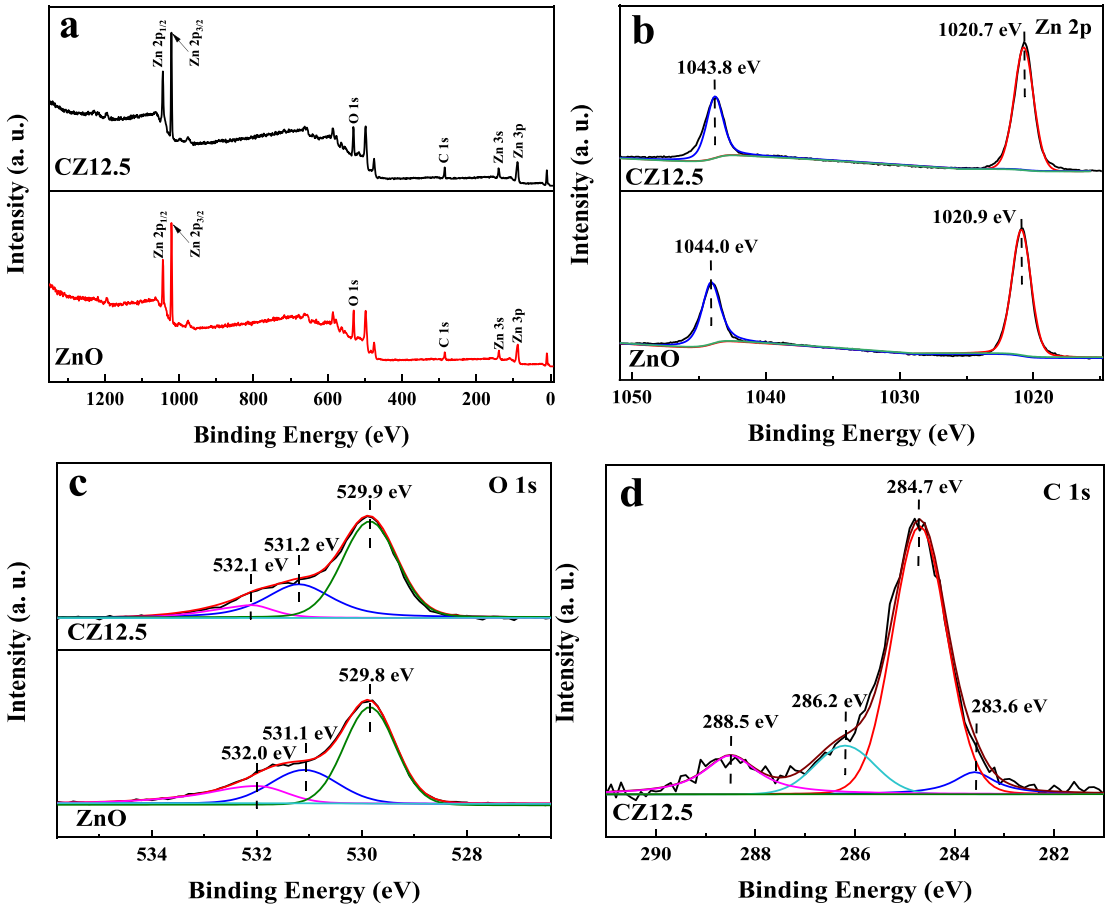

Figure 4. XPS survey spectra (a) of ZnO nanoparticles and CZ12.5 and the corresponding high-resolution XPS spectra (b–d) of Zn 2p (b), O 1s (c), and C 1s (d).

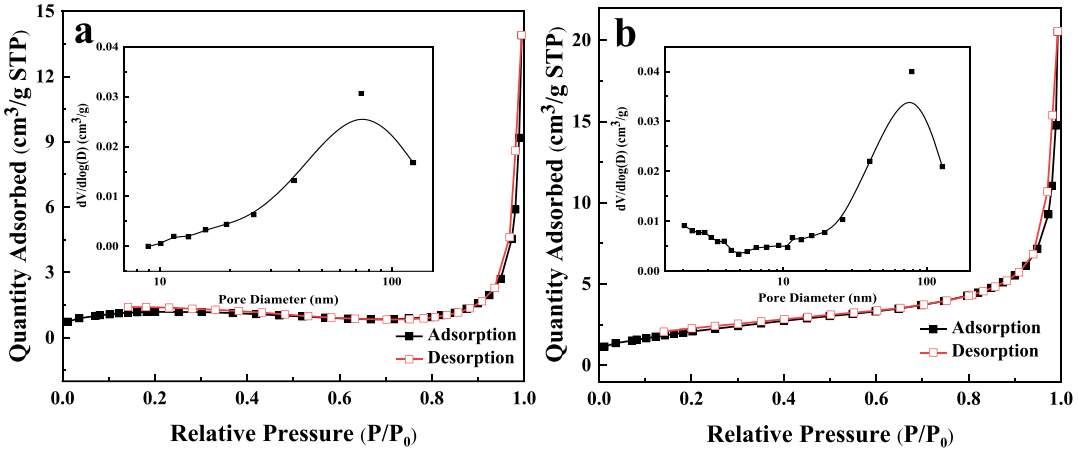

Figure 5. N_2 adsorption–desorption isotherms and the pore size distribution (inset) of ZnO nanoparticles (a) and CZ12.5 (b).

lead to low light absorption for too high content CQDs in the composites.[56] Therefore, the CZ7.5 displays the strongest light absorption capacity.

The band gap energy of a semiconductor is the minimum luminous energy which supplies electrical conductivity. Based on the Kubelka–Munk function[67] from the Tauc plot (Figure 6b), the corresponding band gaps (E_g) of the ZnO nanoparticles and CZ12.5 are measured as 3.20 and 3.10 eV, respectively. For CZ12.5, the low band gap means that solar energy can be utilized more fully, which is due to the introduction of the CQDs in ZnO.

It is known that the charge transfer and separation process are crucial for the photodegradation reaction. The PL technology is often used for the investigation of the recombination efficiency of photoexcited e^-–h^+ pairs, and the weak PL peak intensity means low recombination efficiency. The PL spectra of ZnO and CZ12.5 exhibit an obvious broad PL peak at about 608 nm belonging to ZnO (Figure 7a).[18] Both ZnO nanoparticles and CZ12.5 exhibit a

https://doi.org/10.1021/acsomega.2c07591
ACS Omega 2023, 8, 7845–7857

Table 1. BET Results of ZnO Nanoparticles and the CQDs/ZnO Composites

Sample	S_{BET} ($m^2 \cdot g^{-1}$)	Avg pore volume ($cm^3 \cdot g^{-1}$)	Avg pore size (nm)
ZnO	4.22	0.020	58.58
CZ7.5	4.26	0.028	61.34
CZ10	5.47	0.026	49.20
CZ12.5	7.87	0.032	12.67
CZ15	7.92	0.037	18.29
CZ17.5	8.79	0.035	14.83

similar PL curve shape, suggesting that the modification of CQDs will not produce the new PL responses.[68] The CZ12.5 sample with a weaker PL emission may inhibit recombination of charges and reserve more electrons for photocatalytic reaction from the charge transfer between CQDs and ZnO.[69,70]

The CQDs were detected by PL technology in the excitation wavelength range from 550 to 900 nm (Figure 7b). The CQD solution can emit short wavelength light at a long excitation wavelength, displaying obvious up-conversion luminescence. The emission peak intensity of the CQD solution increases first and then weakens with the increasing excitation wavelength. When the excitation wavelength is less than 650 nm, the CQD solution can emit short wavelength light lower than 400 nm, which is further applied to excite ZnO to obtain more electron−hole pairs. Therefore, the modification of CQDs is very beneficial to increase the light absorption.

To further evaluate the recombination of photogenerated electrons and holes, the TRPL measurements of the ZnO nanoparticles and CZ12.5 were conducted and are shown in Figure 7c. The TRPL decay curves can be well-fitted via a triexponential function.[71] The emission lifetime (τ) is τ_1, τ_2, and τ_3. τ_1 relates to the radiative recombination of e^-−h^+, and τ_2 and τ_3 are caused by the nonradiative recombination of trapping and transferring electrons.[72] The lifetime parameters are summarized in Table 2. Further, the average lifetime (τ_{avg}) of ZnO nanoparticles and CZ12.5 is 5.642 and 5.249 ns, respectively, which is consistent with the above PL results. The fluorescence lifetime of CZ12.5 is shortened compared to ZnO nanoparticles, indicating that CZ12.5 has slower charge recombination, which should be attributed to an effective electron transport[73,74] from the modification of CQDs, which is advantageous for the charge separation.

3.3. Photocatalytic Performance. The photocatalytic degradation of RhB over various photocatalysts was carried out under the illumination of a 300 W Xe lamp (λ > 420 nm). It can be found in Figure 8a that the RhB is hardly removed without catalyst, indicating that RhB will not undergo self-degradation. When the CZ12.5 was used as photocatalyst, only 22% of RhB is removed without illumination. The above control experiments show that both catalyst and illumination are indispensable for the RhB removal. The degradation curves of RhB over various photocatalysts were shown in Figure S2, indicating that the RhB can be effectively removed in the presence of the CQDs/ZnO composites. The photocatalytic degradation of RhB shows a rapid increase and then tends to be stable with the extension of illumination time. The CQDs/ZnO composites show the enhanced photodegradation of RhB with an increasing and then decreasing trend as the increasing content of the CQDs under the irradiation of 30 min. And the CZ12.5 can decompose more RhB molecules with the removal of 99% of them.

According to the quasi-first-order Langmuir−Hinshelwood (L−H) mode,[75−77] the photocatalytic simulation kinetic curve can be obtained by $\ln(C_0/C_t) = k_{app}t$, where k_{app} represents the apparent rate constant.[78] It is found in Figure 8b that the k_{app} value of the CQDs/ZnO composites obviously exceeds that of the ZnO nanoparticles. Moreover, the CZ12.5 possesses the largest k_{app} of 0.1781 min^{-1}, which is 2.6 times that of the ZnO nanoparticles. According to BET specific surface area (Table 1) and the k_{app} value (Figure 8b), the specific catalytic rates of various photocatalysts are listed in Table S1. The specific catalytic rates first increase and then decrease with the CQDs amount in the composites, and the CZ12.5 has the largest specific catalytic rate of 0.0226 $min^{-1} \cdot m^{-2}$. Therefore, the modification of ZnO nanoparticles by CQDs can help to enhance its photocatalytic performance.

In comparison of the as-obtained CQDs/ZnO composite, the photocatalytic performance of RhB over the ZnO-based photocatalysts modified by carbon-containing materials is shown in Table S2. Although various photocatalysts can remove the RhB under their own catalytic conditions, only a few catalysts achieve efficient removal of RhB under visible light. Therefore, the as-obtained CQDs/ZnO composite can display the excellent removal of RhB, meaning the potential application in the removal of synthetic pigment pollutants.

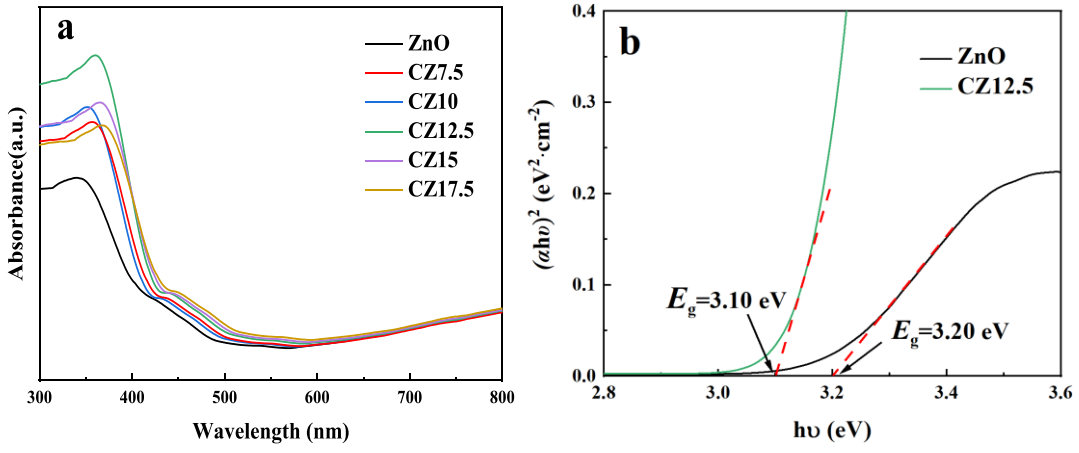

Figure 6. UV−vis DRS (a) and Tauc plots (b) of ZnO nanoparticles and the CQDs/ZnO composites.

https://doi.org/10.1021/acsomega.2c07591
ACS Omega 2023, 8, 7845−7857

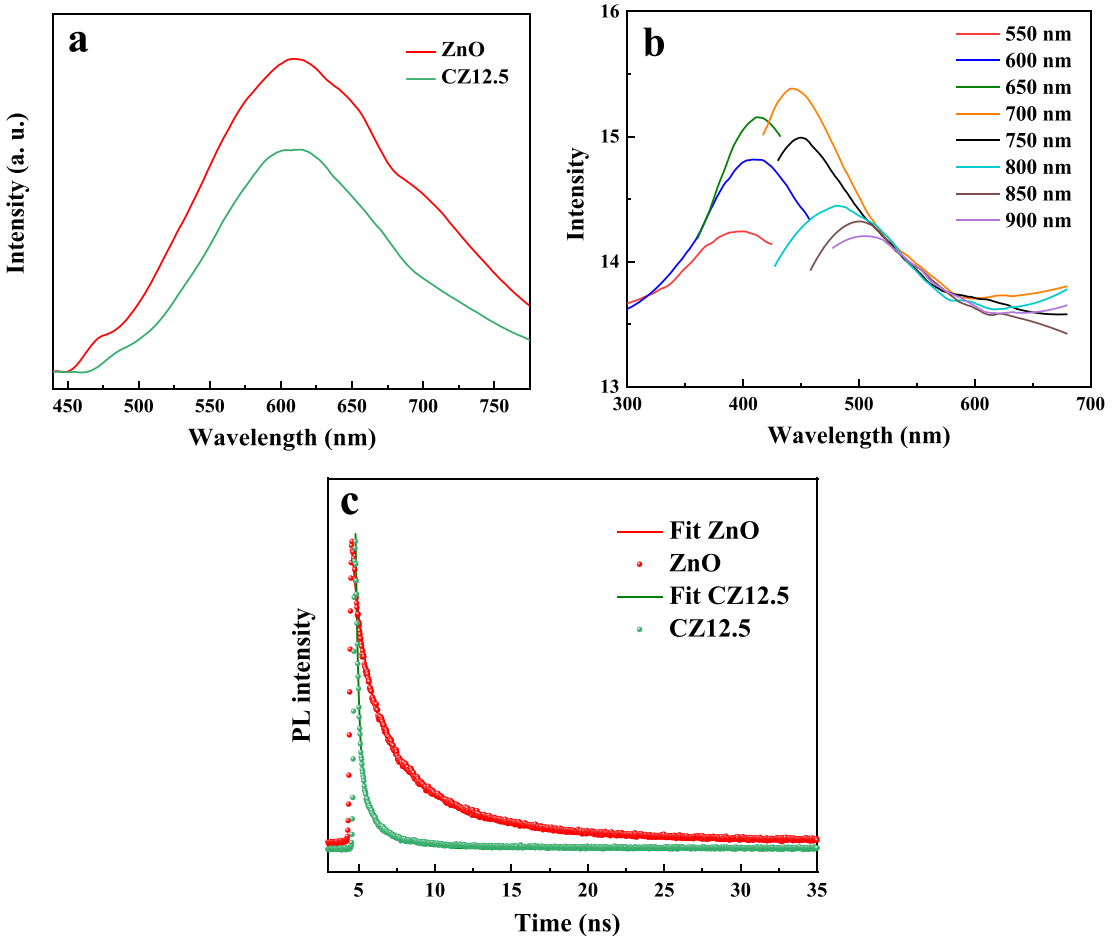

Figure 7. PL spectra of ZnO nanoparticles and CZ12.5 (a) and CQDs (b), and TRPL decay curves (c) of ZnO nanoparticles and CZ12.5 at an excitation wavelength of 405 nm.

Table 2. TRPL Decay Rate of ZnO Nanoparticles and CZ12.5

Sample	τ_1 (ns)	B_1 (%)	τ_2 (ns)	B_2 (%)	τ_3 (ns)	B_3 (%)	τ_{avg} (ns)
ZnO	6.505	52.79	1.527	~0	1.524	47.21	5.642
CZ12.5	6.468	28.91	1.089	44.47	0.197	26.62	5.249

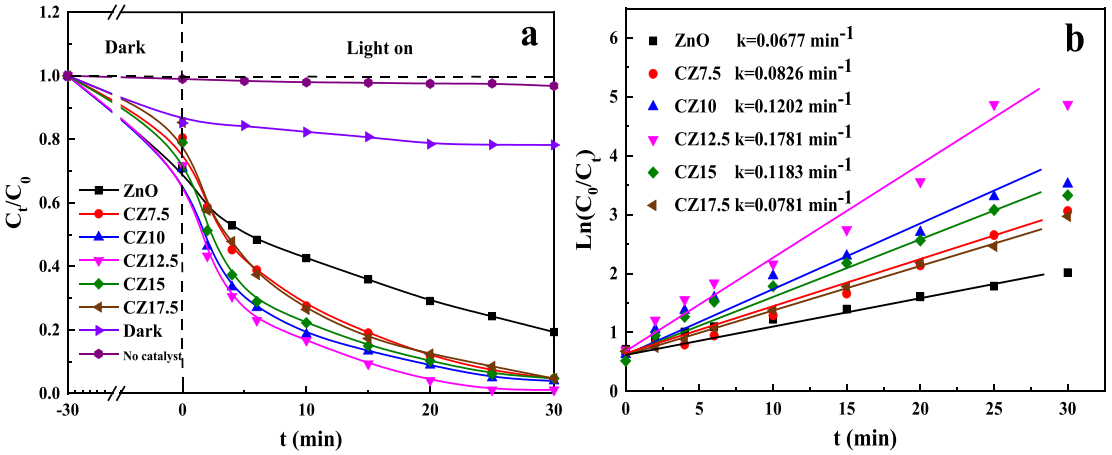

Figure 8. Photocatalytic activities (a) of RhB and kinetic curves (b) over various samples.

Reusability is an important reference to evaluate the practical application of photocatalysts. The CZ12.5 is reused to decompose the RhB molecules under irradiation in Figure 9. After 5 cycles, the RhB solution can still be effectively removed over CZ12.5, and the degradation of RhB still maintains 92%, close to 93% of the first removal efficiency of RhB. At addition,

https://doi.org/10.1021/acsomega.2c07591
ACS Omega 2023, 8, 7845−7857

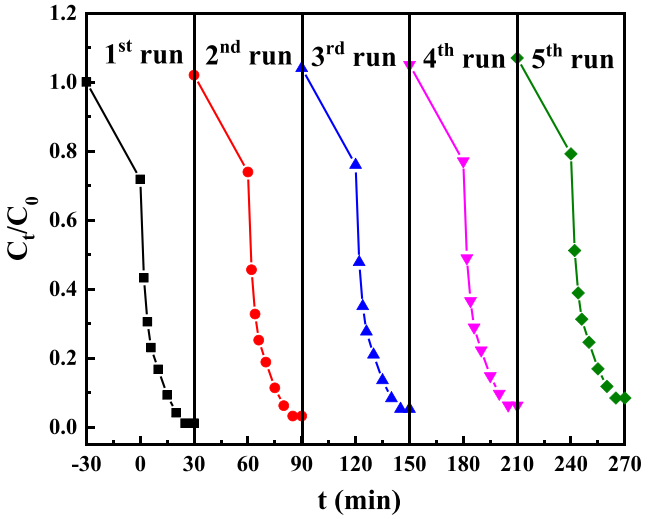

Figure 9. Five cycles of photocatalytic degradation of RhB over CZ12.5.

the reused CZ12.5 after 5 cycles shows XPS spectra similar to those of the unused CZ12.5 (Figure S3), proving that the photodegradation of RhB does not affect the surface composition and elemental valence of the composite. It proves that the ZnO nanoparticles modified by CQDs have excellent stability and recycle ability, which is helpful for practical application.

In order to investigate the universality of the CQDs/ZnO composite, the photodegradation performance of other synthetic pigment pollutants was investigated in Figure S4. At the same experimental conditions, the removal of various pollutants in the presence of the CZ12.5 is more than 85%, which is obviously higher than that in the presence of the ZnO nanoparticles. The above results show the CQDs/ZnO composite has excellent universality and potential application in the removal of synthetic pigment pollutants.

3.4. Photoelectrochemical Properties. The charge separation irradiated by light can be further investigated by the photoelectrochemical experiments, such as transient photocurrent response and electrochemical impedance spectroscopy (EIS) analysis. Figure 10a shows the transient photocurrent responses of various samples that are measured for several "on−off" light cycles. The CQDs/ZnO composites show the higher photocurrent responses than the ZnO nanoparticles. The photocurrent intensity of the composite first goes up and then down along with the continuous addition of CQDs, and the CZ12.5 has the highest photocurrent response. It may be due to the fact that the excessive CQDs could cover the reaction active sites and/or act as the recombination center of charges.[79] The EIS spectra of the ZnO nanoparticles and CZ12.5 were recorded to evaluate the charge transfer and separation with and without light irradiation (Figure 10b). A smaller arc radius represents a lower charge transfer resistance and the higher interface charge separation.[80,81] Both the ZnO nanoparticles and the CZ12.5 have the smaller arc radius under irradiation than under no light, indicating the fast charge transfer under irradiation. The CZ12.5 has a smaller arc radius than that of the ZnO nanoparticles in the cases of irradiation or dark, suggesting its low charge-transfer resistance. Therefore, the modification of CQDs can develop the charge transfer and separation, thereby enhancing the photocatalytic properties.

3.5. Photocatalytic Mechanism. To make clear the photocatalytic mechanism, the active radicals in the photodegradation of RhB were investigated by the trapping experiments. Generally speaking, $^{\bullet}OH$, $^{\bullet}O_2^-$, and h^+ are detected by TBA, BQ, and EDTA-2Na, respectively.[82] With the addition of BQ, the RhB removal is severely prevented and only 19% of RhB was degraded in Figure 11a, indicating that the $^{\bullet}O_2^-$ is the main active substance. It is further proved by the experiments in a pure O_2 condition and a non-O_2 condition replaced by pure N_2 that the O_2 molecules are involved in the reaction. Using EDTA-2Na as a trapping reagent, the RhB degradation with the removal of 22% is also obviously prohibited. In addition, TBA displays an effect on the photocatalytic reaction of RhB and 63% of RhB is decomposed. Therefore, $^{\bullet}O_2^-$ and h^+ are the main active species, and $^{\bullet}OH$ has an impact on the photocatalytic degradation process of RhB.

To further investigate the generation of $^{\bullet}O_2^-$ and $^{\bullet}OH$, NBT and TA molecular probe experiments were put into effect. The absorption peak of NBT at about 259 nm[48] becomes weak in intensity under irradiation due to the reaction between NBT and $^{\bullet}O_2^-$ in Figure 11b, suggesting the generation of $^{\bullet}O_2^-$ during the degradation. The PL response

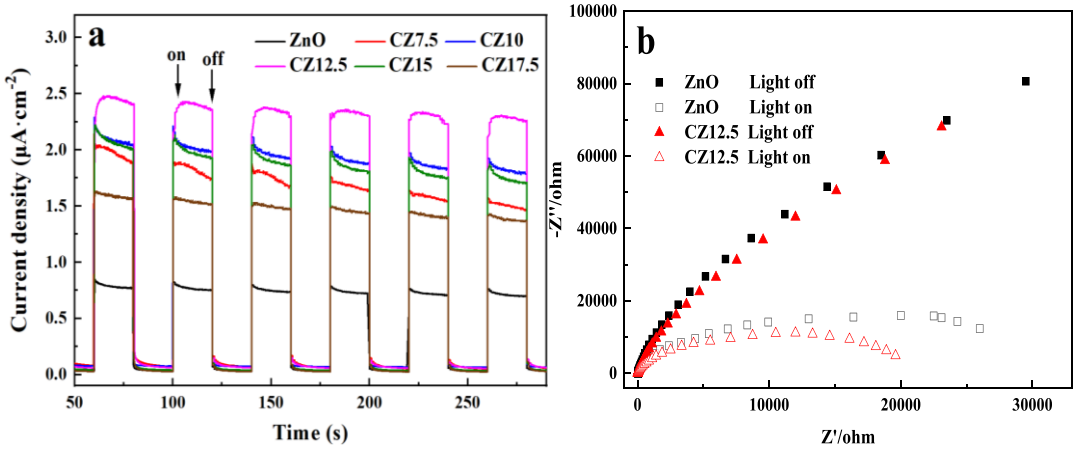

Figure 10. Transient photocurrent response (a) of various samples and EIS Nyquist plots (b) of the ZnO nanoparticles and CZ12.5 with and without light.

https://doi.org/10.1021/acsomega.2c07591
ACS Omega 2023, 8, 7845−7857

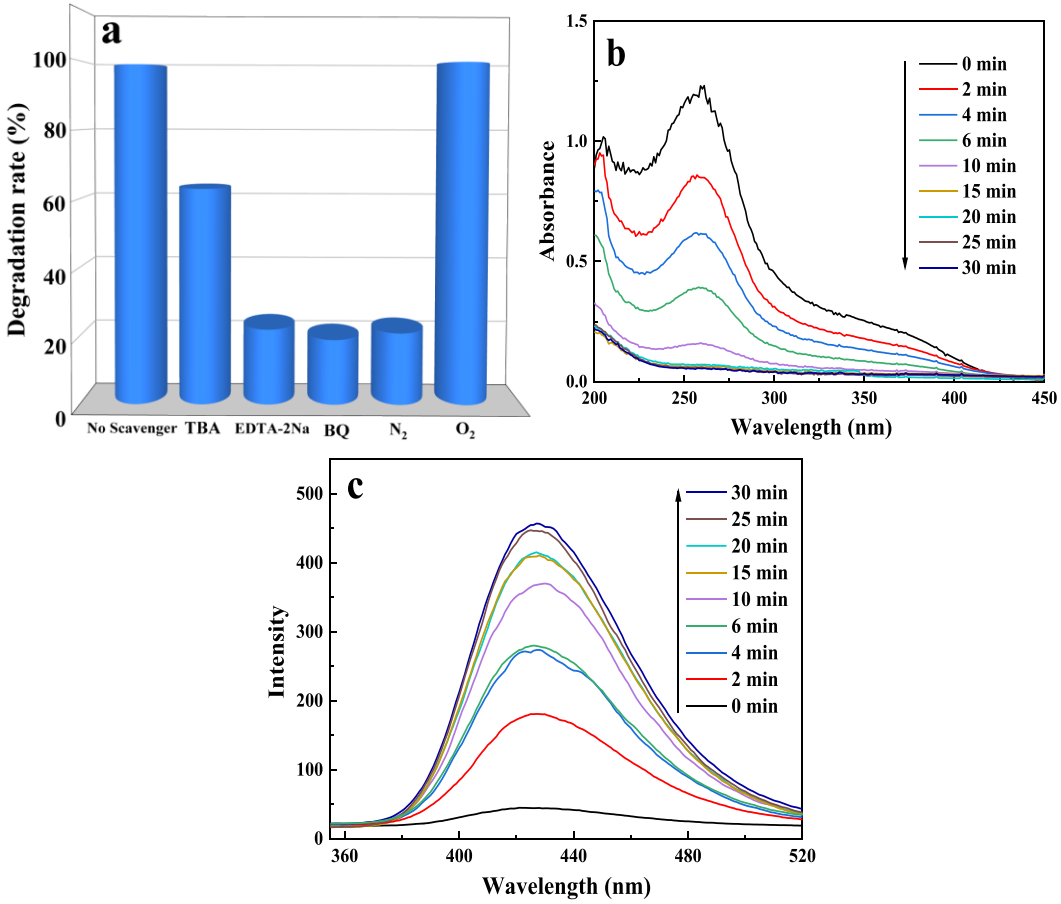

Figure 11. Trapping experiments of active species (a) for the RhB removal over CZ12.5 under irradiation, UV−vis spectra of NBT (b) and PL spectra of HTA (c) over CZ12.5 under excitation wavelength of 300 nm.

of the reaction product of TA and •OH was recorded for monitoring •OH radicals, as shown in Figure 11c. The reaction of TA with •OH radicals can produce the product of HTA, which has a strong fluorescence peak at 425 nm.[49] The enhancement of the PL peak intensity as irradiation time confirms that •OH radicals produced by h^+ are very important for the RhB degradation.[83] The above results are well matched to the trapping experimental results.

After the RhB solution was irradiated under visible light in the presence of CZ12.5, the clear solution obtained by centrifugation was analyzed by the COD removal efficiency to make clear the RhB degradation. According to Figure S5, the COD removal efficiency of RhB gradually decreases with increasing irradiation time. Under the illumination of 30 min, the COD removal of RhB is 82%, while about 99% of RhB has been degraded, indicating the incomplete mineralization. By analyzing the above results, it is speculated that the photocatalytic degradation of RhB may be as follows. First, the chromogenic groups of RhB molecules are destroyed, resulting in the formation of colorless organic intermediates. This is manifested as a rapid decrease in solution chromaticity, leading to the decrease of the degradation efficiency. Then the colorless intermediates were further degraded. According to the degradation curves of RhB over CZ12.5 (Figure S2d), the maximum absorption peak of RhB is slightly blue-shifted, indicating that the deethylation reaction is predominant during the photocatalytic degradation process,[84] while the oxidation of the ring-opening reaction of the benzene ring occupies a secondary position. However, the degradation process of RhB is very complex and the reaction mechanism is not clear.

To further understand the mechanism for the enhanced photocatalytic performance, the property of the band structure was inevitably studied. As shown in Figure S6a, the positive slope of the tangent indicates that the ZnO nanoparticles belong to n-type semiconductor. The flat band position (E_f) of the ZnO nanoparticles can be determined to −0.57 V (vs Ag/AgCl) from the linear potential plots on the basis of the Mott−Schottky (M−S) curves. The E_f value of the ZnO nanoparticles relative to a normal hydrogen electrode (NHE) is 0.043 V (vs NHE) using the formula $E_{NHE} = E_{(Ag/AgCl)}^{\theta} + 0.0591 \times pH + E_{(Ag/AgCl)}$,[85,86] where $E_{(Ag/AgCl)}^{\theta}$ is 0.1989 eV and the pH value is 7. The valence band (VB) of the ZnO nanoparticles from Figure S6b is 2.69 V (vs NHE) The conduction band (CB) of the ZnO nanoparticles can be acquired to be −0.51 V (vs NHE) by the formula $E_{CB} = E_{VB} - E_g$.

The photocatalytic mechanism of RhB over the CQDs/ZnO composite is proposed and illustrated in Figure 12. The CQDs/ZnO samples exhibit the strong light absorption and the enhanced photodegradation of RhB due to the introduction of CQDs in ZnO. First, the carbon atoms from the CQDs come into the ZnO lattice, leading to a new energy level above the VB of ZnO through the hybridization of O 2p and C 2p orbitals.[87] The narrowed band gap of the composite can promote light absorption and enhance the removal of RhB. Second, the electrons on the CQDs produced by visible light can jump to the CB of ZnO. The electrons on the CB of ZnO

https://doi.org/10.1021/acsomega.2c07591
ACS Omega 2023, 8, 7845−7857

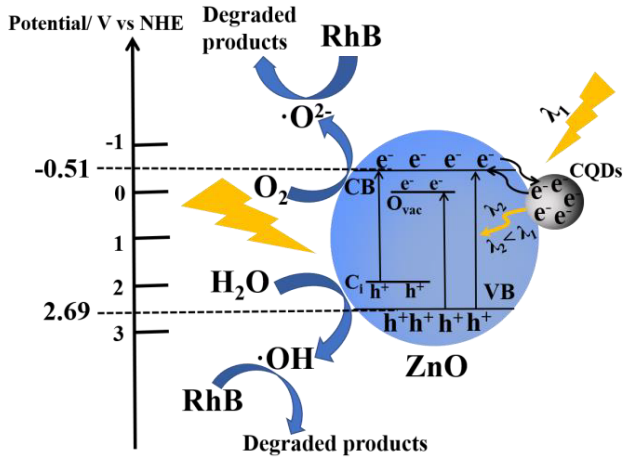

Figure 12. Possible photodegradation mechanism of RhB over the CQDs/ZnO composite.

and the O_{vac} energy level combine with O_2 to form the $^{\bullet}O_2^-$ radicals that decompose the RhB molecules. Third, the CQDs in the composite may act as an electron reservoir to trap electrons from ZnO, thereby enhancing the charge separation. Fourth, the CQDs with up-conversion luminescence can utilize long wavelength light to emit light below 400 nm that further excites ZnO to generate more electrons.[36] Due to a more positive VB, the photogenerated holes on the VB of ZnO and the energy level of carbon dopants react with H_2O to produce $^{\bullet}OH$ that can degrade RhB. Therefore, the CQDs/ZnO composite can produce the more photoexcited electrons and holes, inhibit the charge recombination, thereby enhancing the photodegradation of RhB.

DMPO spin-trapping ESR spectra were employed to further detect the active groups of $^{\bullet}O_2^-$ and $^{\bullet}OH$ radicals during the RhB photodegradation. As shown in Figure S7, no peaks can be observed in the darkness. Under the irradiation the strong signals of $^{\bullet}O_2^-$ and $^{\bullet}OH$ radicals can be measured, indicating the generation of $^{\bullet}O_2^-$ and $^{\bullet}OH$ radicals in the photoreaction.[88] This is consistent with the speculated mechanism of the RhB photodegradation.

4. CONCLUSIONS

The biomass-derived CQDs were effectively fabricated by using shaddock peel as the carbon source. The ZIF-8 derived ZnO nanoparticles modified by different content of CQDs were successfully constructed via a solvothermal process, which is low-cost and facile for the formation of the interface interaction between CQDs and ZnO nanoparticles. The combined action of the structure of the CQDs/ZnO composite and the modification of CQDs promote the wide photoresponse range, low fluorescent PL intensity, high charge transfer efficiency, and small transfer resistance of charge carriers, which promotes more high separation efficiency of charges. Thus, the CQDs/ZnO composites exhibit better catalytic activity and higher cycle stability of RhB than ZnO nanoparticles under visible light. The present study provides an effective method to construct the visible-light-responsive ZnO-based photocatalyst with excellent catalytic properties and high stability, which displays the potential applications in the removal of synthetic pigment pollutants in the food industry.

ASSOCIATED CONTENT

Supporting Information

The Supporting Information is available free of charge at https://pubs.acs.org/doi/10.1021/acsomega.2c07591.

PRL data fitting details, SEM images of ZnO nanoparticles and CZ12.5, degradation curves of RhB over ZnO nanoparticles and the CQDs/ZnO composites, comparison of the specific catalytic efficiency over various photocatalysts on the RhB degradation, comparison of the photocatalytic performance of RhB over various ZnO-based photocatalysts modified by carbon-containing materials, XPS survey spectra and the corresponding high-resolution XPS spectra, degradation performance of various synthetic pigment pollutants over CZ12.5 and ZnO nanoparticles, COD removal of RhB over CZ12.5, M-S plots and VB-XPS spectrum of ZnO nanoparticles, and DMPO spin-trapping ESR spectra for $\cdot O_2^-$ and ·OH radicals over CZ12.5 (PDF)

AUTHOR INFORMATION

Corresponding Author

Fei-Fei Tao − *Department of Chemistry and Chemical Engineering, Shaoxing University, Zhejiang 312000, P.R. China;* orcid.org/0000-0003-4243-8759; Email: feifeitao@usx.edu.cn; Fax: +86-575-88342505

Authors

Jing-Jing Xu − *Department of Chemistry and Chemical Engineering, Shaoxing University, Zhejiang 312000, P.R. China;* orcid.org/0000-0001-7469-5368

Yi-Ning Lu − *Department of Chemistry and Chemical Engineering, Shaoxing University, Zhejiang 312000, P.R. China;* orcid.org/0000-0003-1282-558X

Peng-Fei Liang − *Department of Chemistry and Chemical Engineering, Shaoxing University, Zhejiang 312000, P.R. China;* orcid.org/0000-0002-9016-0942

Ping-An Zhang − *Department of Chemistry and Chemical Engineering, Shaoxing University, Zhejiang 312000, P.R. China*

Complete contact information is available at: https://pubs.acs.org/10.1021/acsomega.2c07591

Author Contributions

F.-F.T. conceived the research project. J.-J.X. performed the experiments and the data preparation. F.-F.T. J.-J.X. and P.-A.Z. wrote the draft, revision, and editing. Y.-N.L. and P.-F.L. performed the figure creation. All authors contributed to the interpretation of the data.

Notes

The authors declare no competing financial interest.

ACKNOWLEDGMENTS

This work was supported by the National Natural Science Foundation of China (NSFC, Grant No. 51372154 and 20901051) and by the Zhejiang Provincial Natural Science Foundation of China under Grant No. LY21B010005. The authors thank Tong Li (Department of Chemistry and Chemical Engineering, Shaoxing University) for the help in the synthesis of the photocatalysts.

REFERENCES

(1) Tran-Truc-Phuong, N.; Xoan-Hoang, T.; La-Ngoc-Tran, N.; Gia-Phuc, L.; Phung, V.-D.; Kieu-Thi Ta, H.; Ngoc-Bach, T.; Hoa-Thi-Tran, N.; The-Loan-Trinh, K. Rapid and sensitive detection of Rhodamine B in food using the plasmonic silver nanocube-based sensor as SERS active substrate. *Spectrochim. Acta, Part A* **2021**, *263*, 120179.

(2) Wang, M.; Nie, X.; Tian, L.; Hu, J.; Yin, D.; Qiao, H.; Li, T.; Li, Y. Rhodamine B in spices determined by a sensitive UPLC-MS/MS method. *Food Addit. Contam, Part B* **2019**, *12*, 59−64.

(3) Han, Q.; Yang, Z.; Wang, L.; Shen, Z.; Wang, X.; Zhu, J.; Jiang, X. An ion exchange strategy to BiOI/CH_3COO(BiO) heterojunction with enhanced visible-light photocatalytic activity. *Appl. Surf. Sci.* **2017**, *403*, 103−111.

(4) Wang, C.-Y.; Zeng, W.-J.; Jiang, T.-T.; Chen, X.; Zhang, X.-L. Incorporating attapulgite nanorods into graphene oxide nanofiltration membranes for efficient dyes wastewater treatment. *Sep. Purif. Technol.* **2019**, *214*, 21−30.

(5) Bethi, B.; Manasa, V.; Srinija, K.; Sonawane, S. H. Intensification of Rhodamine-B dye removal using hydrodynamic cavitation coupled with hydrogel adsorption. *Chem. Eng. Process* **2018**, *134*, 51−57.

(6) Guo, Y.; Zhou, C.; Fang, L.; Liu, Z.; Li, W.; Yang, M. Effect of pH on the catalytic degradation of Rhodamine B by synthesized CDs/g-C_3N_4/Cu_xO composites. *ACS Omega* **2021**, *6*, 8119−8130.

(7) Fu, Y.; Ren, Z.; Wu, J.; Li, Y.; Liu, W.; Li, P.; Xing, L.; Ma, J.; Wang, H.; Xue, X. Direct Z-scheme heterojunction of ZnO/MoS_2 nanoarrays realized by flowing-induced piezoelectric field for enhanced sunlight photocatalytic performances. *Appl. Catal., B* **2021**, *285*, 119785.

(8) Fujishima, A.; Honda, K. Electrochemical photolysis of water at a semiconductor electrode. *Nature* **1972**, *238*, 37.

(9) Qu, R.; Liu, N.; Chen, Y.; Zhang, W.; Zhu, G.; Zhang, Q.; Feng, L. Morphology-induced TiO_2 bandgap change for super rapid treatment of dye wastewater under visible light. *Adv. Mater. Technol.* **2017**, *2*, 1700125.

(10) Silveira, J. V.; Moraes, E. C.; Moura, J. V. B.; Ghosh, A.; Senna, C. A.; Archanjo, B. S.; Vasconcelos, T. L.; Souza-Filho, A. G.; Freire, P. T. C.; Luz-Lima, C. Mo-doped WO_3 nanowires for adsorbing methylene blue dye from wastewater. *J. Mater. Sci.* **2020**, *55*, 6429−6440.

(11) Wang, Y.; Cao, Y.; Liu, Y.; Yang, P. Effect of nonmetal element dopants on photo- and electro-chemistry performance of ultrathin g-C_3N_4 nanosheets. *Int. J. Hydrogen Energy* **2020**, *45*, 16519−16527.

(12) Wang, C.; Luo, S.; Liu, C.; Liu, X.; Chen, C. Photocatalytic performance of single crystal ZnO nanorods and ZnO nanorods films under natural sunlight. *Inorg. Chem. Commun.* **2020**, *114*, 107842.

(13) Gavade, N. L.; Kadam, A. N.; Babar, S. B.; Gophane, A. D.; Garadkar, K. M.; Lee, S.-W. Biogenic synthesis of gold-anchored ZnO nanorods as photocatalyst for sunlight-induced degradation of dye effluent and its toxicity assessment. *Ceram. Int.* **2020**, *46*, 11317−11327.

(14) Gnanasekaran, L.; Santhamoorthy, M.; Naushad, M.; ALOthman, Z. A.; Soto-Moscoso, M.; Show, P. L.; Khoo, K. S. Photocatalytic removal of food colorant using NiO/CuO heterojunction nanomaterials. *Food Chem. Toxicol.* **2022**, *167*, 113277.

(15) Alamgir; Talha, K.; Wang, Y. J.; Ullah, R.; Wang, B.; Wang, L.; Wu, W.; Chen, S.; Xie, L. H.; Li, J. R. Construction of a mixed ligand MOF as "green catalyst" for the photocatalytic degradation of organic dye in aqueous media. *RSC Adv.* **2021**, *11*, 23838−23845.

(16) Hu, C.; Liu, Z.-T.; Yang, P.-C.; Ding, Y.-X.; Lin, K.-Y. A.; Nguyen, B.-S. Self-assembly L-cysteine based 2D g-C_3N_4 nanoflakes for light-dependent degradation of rhodamine B and tetracycline through photocatalysis. *J. Taiwan Inst. Chem. Eng.* **2021**, *123*, 219−227.

(17) Sun, C.; Fu, Y.; Wang, Q.; Xing, L.; Liu, B.; Xue, X. Ultrafast piezo-photocatalytic degradation of organic pollutions by Ag_2O/tetrapod-ZnO nanostructures under ultrasonic/UV exposure. *RSC Adv.* **2016**, *6*, 87446−87453.

(18) Song, S.; Wu, K.; Wu, H.; Guo, J.; Zhang, L. Multi-shelled ZnO decorated with nitrogen and phosphorus co-doped carbon quantum dots: synthesis and enhanced photodegradation activity of methylene blue in aqueous solutions. *RSC Adv.* **2019**, *9*, 7362−7374.

(19) Sharma, S.; Mehta, S. K.; Kansal, S. K. N doped ZnO/C-dots nanoflowers as visible light driven photocatalyst for the degradation of malachite green dye in aqueous phase. *J. Alloys Compd.* **2017**, *699*, 323−333.

(20) Zhao, K.; Yan, X.; Gu, Y.; Kang, Z.; Bai, Z.; Cao, S.; Liu, Y.; Zhang, X.; Zhang, Y. Self-powered photoelectrochemical biosensor based on CdS/RGO/ZnO nanowire array heterostructure. *Small* **2016**, *12*, 245−251.

(21) Zhu, L.; Li, H.; Liu, Z.; Xia, P.; Xie, Y.; Xiong, D. Synthesis of the 0D/3D CuO/ZnO heterojunction with enhanced photocatalytic activity. *J. Phys. Chem. C* **2018**, *122*, 9531−9539.

(22) Li, J.; Liu, K.; Xue, J.; Xue, G.; Sheng, X.; Wang, H.; Huo, P.; Yan, Y. CQDs preluded carbon-incorporated 3D burger-like hybrid ZnO enhanced visible-light-driven photocatalytic activity and mechanism implication. *J. Catal.* **2019**, *369*, 450−461.

(23) Wang, S.; Zhang, X.; Li, S.; Fang, Y.; Pan, L.; Zou, J. J. C-doped ZnO ball-in-ball hollow microspheres for efficient photocatalytic and photoelectrochemical applications. *J. Hazard. Mater.* **2017**, *331*, 235−245.

(24) Koppala, S.; Xia, Y.; Zhang, L.; Peng, J.; Chen, Z.; Xu, L. Hierarchical ZnO/Ag nanocomposites for plasmon-enhanced visible-light photocatalytic performance. *Ceram. Int.* **2019**, *45*, 15116−15121.

(25) Al-Haddad, M.; Shawky, A.; Mkhalid, I. A. Highly active ZIF-8 derived CuO@ZnO p-n heterojunction nanostructures for fast visible-light-driven photooxidation of antibiotic waste in water. *J. Taiwan Inst. Chem. Eng.* **2021**, *123*, 284−292.

(26) Oliveira, J. A.; Nogueira, A. E.; Gonçalves, M. C. P.; Paris, E. C.; Ribeiro, C.; Poirier, G. Y.; Giraldi, T. R. Photoactivity of N-doped ZnO nanoparticles in oxidative and reductive reactions. *Appl. Surf. Sci.* **2018**, *433*, 879−886.

(27) Andrade, G. R. S.; Nascimento, C. C.; Lima, Z. M.; Teixeira-Neto, E.; Costa, L. P.; Gimenez, I. F. Star-shaped ZnO/Ag hybrid nanostructures for enhanced photocatalysis and antibacterial activity. *Appl. Surf. Sci.* **2017**, *399*, 573−582.

(28) Kumari, V.; Mittal, A.; Jindal, J.; Yadav, S.; Kumar, N. S-,N- and C-doped ZnO as semiconductor photocatalysts: A review. *Front. Mater. Sci.* **2019**, *13*, 1−22.

(29) Jia, X.; Li, J.; Wang, E. One-pot green synthesis of optically pH-sensitive carbon dots with upconversion luminescence. *Nanoscale* **2012**, *4*, 5572.

(30) Xia, J.; Di, J.; Li, H.; Xu, H.; Li, H.; Guo, S. Ionic liquid-induced strategy for carbon quantum dots/BiOX (X = Br, Cl) hybrid nanosheets with superior visible light-driven photocatalysis. *Appl. Catal., B* **2016**, *181*, 260−269.

(31) Zirak, M.; Alehdaghi, H.; Shakoori, A. M. Preparation of ZnO-carbon quantum dot composite thin films with superhydrophilic surface. *Mater. Technol.* **2021**, *36*, 72−80.

(32) Gu, X.; Yan, Q.; Wei, Y.; Luo, Y.; Sun, Y.; Zhao, D.; Ji, F.; Xu, X. Visible-light-responsive photocatalyst with a microsphere structure: preparation and photocatalytic performance of CQDs@BiOCl. *J. Mater. Sci.: Mater. Electron.* **2019**, *30*, 16321−16336.

(33) Qu, Y.; Xu, X.; Huang, R.; Qi, W.; Su, R.; He, Z. Enhanced photocatalytic degradation of antibiotics in water over functionalized N,S-doped carbon quantum dots embedded ZnO nanoflowers under sunlight irradiation. *Chem. Eng. J.* **2020**, *382*, 123016.

(34) Li, Y.; Zhang, B.-P.; Zhao, J.-X.; Ge, Z.-H.; Zhao, X.-K.; Zou, L. ZnO/carbon quantum dots heterostructure with enhanced photocatalytic properties. *Appl. Surf. Sci.* **2013**, *279*, 367−373.

(35) Bozetine, H.; Wang, Q.; Barras, A.; Li, M.; Hadjersi, T.; Szunerits, S.; Boukherroub, R. Green chemistry approach for the synthesis of ZnO-carbon dots nanocomposites with good photocatalytic properties under visible light. *J. Colloid Interface Sci.* **2016**, *465*, 286−294.

(36) Ding, D.; Lan, W.; Yang, Z.; Zhao, X.; Chen, Y.; Wang, J.; Zhang, X.; Zhang, Y.; Su, Q.; Xie, E. A simple method for preparing

https://doi.org/10.1021/acsomega.2c07591
ACS Omega 2023, 8, 7845−7857

ZnO foam/carbon quantum dots nanocomposite and their photocatalytic applications. *Mater. Sci. Semicond. Process.* **2016**, *47*, 25−31.
(37) Wang, L.; Ma, C.; Ru, X.; Guo, Z.; Wu, D.; Zhang, S.; Yu, G.; Hu, Y.; Wang, J. Facile synthesis of ZnO hollow microspheres and their high performance in photocatalytic degradation and dye sensitized solar cells. *J. Alloys Compd.* **2015**, *647*, 57−62.
(38) Wu, D.; Wang, Y.; Ma, N.; Cao, K.; Zhang, W.; Chen, J.; Wang, D.; Gao, Z.; Xu, F.; Jiang, K. Single-crystal-like ZnO mesoporous spheres derived from metal organic framework delivering high electron mobility for enhanced energy conversion and storage performances. *Electrochim. Acta* **2019**, *305*, 474−483.
(39) Salari, H.; Sadeghinia, M. MOF-templated synthesis of nano Ag_2O/ZnO/CuO heterostructure for photocatalysis. *J. Photochem. Photobiol., A* **2019**, *376*, 279−287.
(40) Zhang, Y.-N.; Li, B.; Fu, L.; Li, Q.; Yin, L.-W. MOF-derived ZnO as electron transport layer for improving light harvesting and electron extraction efficiency in perovskite solar cells. *Electrochim. Acta* **2020**, *330*, 135280.
(41) Su, Y.; Li, S.; He, D.; Yu, D.; Liu, F.; Shao, N.; Zhang, Z. MOF-derived porous ZnO nanocages/rGO/carbon sponge-based photocatalytic microreactor for efficient degradation of water pollutants and hydrogen evolution. *ACS Sustainable Chem. Eng.* **2018**, *6*, 11989−11998.
(42) Hussain, M. Z.; Yang, Z.; Huang, Z.; Jia, Q.; Zhu, Y.; Xia, Y. Recent advances in metal-organic frameworks derived nanocomposites for photocatalytic applications in energy and environment. *Adv. Sci.* **2021**, *8*, 2100625.
(43) Wang, T.; Wang, Y.; Sun, M.; Hanif, A.; Wu, H.; Gu, Q.; Ok, Y. S.; Tsang, D. C. W.; Li, J.; Yu, J.; Shang, J. Thermally treated zeolitic imidazolate framework-8 (ZIF-8) for visible light photocatalytic degradation of gaseous formaldehyde. *Chem. Sci.* **2020**, *11*, 6670−6681.
(44) Payra, S.; Challagulla, S.; Bobde, Y.; Chakraborty, C.; Ghosh, B.; Roy, S. Probing the photo- and electro-catalytic degradation mechanism of methylene blue dye over ZIF-derived ZnO. *J. Hazard. Mater.* **2019**, *373*, 377−388.
(45) Pan, Y.; Liu, Y.; Zeng, G.; Zhao, L.; Lai, Z. Rapid synthesis of zeolitic imidazolate framework-8 (ZIF-8) nanocrystals in an aqueous system. *Chem. Commun.* **2011**, *47*, 2071−2073.
(46) Wang, M.; Shi, R.; Gao, M.; Zhang, K.; Deng, L.; Fu, Q.; Wang, L.; Gao, D. Sensitivity fluorescent switching sensor for Cr (VI) and ascorbic acid detection based on orange peels-derived carbon dots modified with EDTA. *Food Chem.* **2020**, *318*, 126506.
(47) Cheng, Y.; Wang, X.; Mei, Y.; Wang, D.; Ji, C. ZnCDs/ZnO@ZIF-8 zeolite composites for the photocatalytic degradation of tetracycline. *Catalysts* **2021**, *11*, 934.
(48) Liu, S.-J.; Li, F.-T.; Li, Y.-L.; Hao, Y.-J.; Wang, X.-J.; Li, B.; Liu, R.-H. Fabrication of ternary g-C_3N_4/Al_2O_3/ZnO heterojunctions based on cascade electron transfer toward molecular oxygen activation. *Appl. Catal., B* **2017**, *212*, 115−128.
(49) Lamba, R.; Umar, A.; Mehta, S. K.; Anderson, W. A.; Kansal, S. K. Visible-light-driven photocatalytic properties of self assembled cauliflower-like AgCl/ZnO hierarchical nanostructures. *J. Mol. Catal. A: Chem.* **2015**, *408*, 189−201.
(50) Zhang, X.; Pan, J.; Zhu, C.; Sheng, Y.; Yan, Z.; Wang, Y.; Feng, B. The visible light catalytic properties of carbon quantum dots/ZnO nanoflowers composites. *J. Mater. Sci.: Mater. Electron.* **2015**, *26*, 2861−2866.
(51) Liu, C.; Qiu, Y.; Wang, F.; Li, L.; Liang, Q.; Chen, Z. Electrodeposition of ZnO nanoflake-based photoanode sensitized by carbon quantum dots for photoelectrochemical water oxidation. *Ceram. Int.* **2017**, *43*, 5329−5333.
(52) Zhang, X.; Chen, Y.; Zhang, S.; Qiu, C. High photocatalytic performance of high concentration Al-doped ZnO nanoparticles. *Sep. Purif. Technol.* **2017**, *172*, 236−241.
(53) Wang, H.; Wei, Z.; Matsui, H.; Zhou, S. Fe_3O_4/carbon quantum dots hybrid nanoflowers for highly active and recyclable visible-light driven photocatalyst. *J. Mater. Chem. A* **2014**, *2*, 15740−15745.
(54) Liu, R.; Li, H.; Duan, L.; Shen, H.; Zhang, Y.; Zhao, X. In situ synthesis and enhanced visible light photocatalytic activity of C-TiO_2 microspheres/carbon quantum dots. *Ceram. Int.* **2017**, *43*, 8648−8654.
(55) Di, J.; Xia, J.; Ji, M.; Xu, L.; Yin, S.; Chen, Z.; Li, H. Bidirectional acceleration of carrier separation spatially via N-CQDs/atomically-thin BiOI nanosheets nanojunctions for manipulating active species in a photocatalytic process. *J. Mater. Chem. A* **2016**, *4*, 5051−5061.
(56) Liang, H.; Tai, X.; Du, Z.; Yin, Y. Enhanced photocatalytic activity of ZnO sensitized by carbon quantum dots and application in phenol wastewater. *Opt. Mater.* **2020**, *100*, 109674.
(57) Xiong, G.; Pal, U.; Serrano, J. G.; Ucer, K. B.; Williams, R. T. Photoluminesence and FTIR study of ZnO nanoparticles: the impurity and defect perspective. *Phys. Stat. Sol. C* **2006**, *3*, 3577−3581.
(58) Chen, J.; Chen, Q.; Ma, Q. Influence of surface functionalization via chemical oxidation on the properties of carbon nanotubes. *J. Colloid Interface Sci.* **2012**, *370*, 32−38.
(59) Mukherjee, I.; Cilamkoti, V.; Dutta, R. K. Sunlight-driven photocatalytic degradation of ciprofloxacin by carbon dots embedded in ZnO nanostructures. *ACS Appl. Nano Mater.* **2021**, *4*, 7686−7697.
(60) Zhang, L.; Liang, Q.; Yang, P.; Huang, Y.; Liu, Y.; Yang, H.; Yan, J. ZIF-8 derived ZnO/$Zn_6Al_2O_9$/Al_2O_3 nanocomposite with excellent photocatalytic performance under simulated sunlight irradiation. *New J. Chem.* **2019**, *43*, 2990−2999.
(61) Cui, J.; Wu, D.; Li, Z.; Zhao, G.; Wang, J.; Wang, L.; Niu, B. Mesoporous Ag/ZnO hybrid cages derived from ZIF-8 for enhanced photocatalytic and antibacterial activities. *Ceram. Int.* **2021**, *47*, 15759−15770.
(62) Chang, Y.-C.; Hsu, C.-C. Synergetic effect of carbon black as co-catalyst for enhanced visible-light photocatalytic activity and stability on ZnO nanoparticles. *Solid State Sci.* **2020**, *107*, 106366.
(63) Qin, J.; Yang, C.; Cao, M.; Zhang, X.; Rajendran, S.; Limpanart, S.; Ma, M.; Liu, R. Two-dimensional porous sheet-like carbon-doped ZnO/g-C_3N_4 nanocomposite with high visible-light photocatalytic performance. *Mater. Lett.* **2017**, *189*, 156−159.
(64) Zhang, X.; Qin, J.; Hao, R.; Wang, L.; Shen, X.; Yu, R.; Limpanart, S.; Ma, M.; Liu, R. Carbon-doped ZnO nanostructures: facile synthesis and visible light photocatalytic applications. *J. Phys, Chem. C* **2015**, *119*, 20544−20554.
(65) Liang, P.; Zhang, C.; Sun, H.; Liu, S.; Tadé, M.; Wang, S. Photocatalysis of C, N-doped ZnO derived from ZIF-8 for dye degradation and water oxidation. *RSC Adv.* **2016**, *6*, 95903−95909.
(66) Guo, Y.; Kong, X.; Liang, Z.; Xue, Y.; Cui, H.; Tian, J. Non-high temperature method to synthesize carbon coated TiO_2 nanodendrites for enhanced wide spectrum photocatalytic hydrogen evolution activity. *J. Colloid Interface Sci.* **2020**, *571*, 412−418.
(67) Sharma, S.; Kumar, S.; Arumugam, S. M.; Elumalai, S. Promising photocatalytic degradation of lignin over carbon quantum dots decorated TiO_2 nanocomposite in aqueous condition. *Appl. Catal., A* **2020**, *602*, 117730.
(68) Du, P. D.; Hieu, N. T.; Thien, T. V.; Nguyen, D. T. Ultrasound-assisted rapid ZIF-8 synthesis, porous ZnO preparation by heating ZIF-8, and their photocatalytic activity. *J. Nanomater.* **2021**, *2021*, 1−12.
(69) Qu, Z.; Wang, J.; Tang, J.; Shu, X.; Liu, X.; Zhang, Z.; Wang, J. Carbon quantum dots/$KNbO_3$ hybrid composites with enhanced visible-light driven photocatalytic activity toward dye waste-water degradation and hydrogen production. *Mol. Catal.* **2018**, *445*, 1−11.
(70) Li, T.; Liu, Y.; Li, M.; Jiang, J.; Gao, J.; Dong, S. Fabrication of oxygen defect-rich pencil-like ZnO nanorods with CDots and Ag co-enhanced photocatalytic activity for tetracycline hydrochloride degradation. *Sep. Purif. Technol.* **2021**, *266*, 118605.
(71) Samanta, S.; Satpati, B.; Srivastava, R. Unraveling the impact of the Pd nanoparticle@$BiVO_4$/S-CN heterostructure on the photophysical & opto-electronic properties for enhanced catalytic activity in water splitting and one-pot three-step tandem reaction. *Nanoscale Adv.* **2019**, *1*, 1395−1412.

https://doi.org/10.1021/acsomega.2c07591
ACS Omega 2023, 8, 7845−7857

(72) Zeng, Y.; Liu, X.; Liu, C.; Wang, L.; Xia, Y.; Zhang, S.; Luo, S.; Pei, Y. Scalable one-step production of porous oxygen-doped g-C_3N_4 nanorods with effective electron separation for excellent visible-light photocatalytic activity. *Appl. Catal., B* **2018**, *224*, 1−9.
(73) Jiang, J.; Cao, S.; Hu, C.; Chen, C. A comparison study of alkali metal-doped g-C_3N_4 for visible-light photocatalytic hydrogen evolution. *Chin. J. Catal.* **2017**, *38*, 1981−1989.
(74) Wang, Y.; Li, Y.; Cao, S.; Yu, J. Ni-P cluster modified carbon nitride toward efficient photocatalytic hydrogen production. *Chin. J. Catal.* **2019**, *40*, 867−874.
(75) Tang, W. Z.; An, H. UV/TiO_2 photocatalytic oxidation of commercial dyes in aqueous solutions. *Chemosphere* **1995**, *31*, 4157−4170.
(76) Arabatzis, I. M.; Stergiopoulos, T.; Andreeva, D.; Kitova, S.; Neophytides, S. G.; Falaras, P. Characterization and photocatalytic activity of Au/TiO_2 thin films for azo-dye degradation. *J. Catal.* **2003**, *220*, 127−135.
(77) Li, J.; Luo, D.; Yang, C.; He, S.; Chen, S.; Lin, J.; Zhu, L.; Li, X. Copper (II) imidazolate frameworks as highly efficient photocatalysts for reduction of CO_2 into methanol under visible light irradiation. *J. Solid State Chem.* **2013**, *203*, 154−159.
(78) Messina, M. M.; Coustet, M. E.; Ubogui, J.; Ruiz, R.; Saccone, F. D.; Dos-Santos-Claro, P. C.; Ibañez, F. J. Simultaneous detection and photocatalysis performed on a 3D graphene/ZnO hybrid platform. *Langmuir* **2020**, *36*, 2231−2239.
(79) Xu, D.; Li, L.; He, R.; Qi, L.; Zhang, L.; Cheng, B. Noble metal-free RGO/TiO_2 composite nanofiber with enhanced photocatalytic H_2-production performance. *Appl. Surf. Sci.* **2018**, *434*, 620−625.
(80) Zhu, X.; Wei, Z.; Zhao, W.; Zhang, X.; Zhang, L.; Wang, X. Microstructure and electrochemical properties of $ZnMn_2O_4$ nano-powder synthesized using different surfactants. *J. Electron. Mater.* **2018**, *47*, 6428−6436.
(81) Bai, X.; Wang, L.; Zong, R.; Lv, Y.; Sun, Y.; Zhu, Y. Performance enhancement of ZnO photocatalyst via synergic effect of surface oxygen defect and graphene hybridization. *Langmuir* **2013**, *29*, 3097−3105.
(82) Yang, H.; Xu, B.; Yuan, S.; Zhang, Q.; Zhang, M.; Ohno, T. Synthesis of Y-doped CeO_2/PCN nanocomposited photocatalyst with promoted photoredox performance. *Appl. Catal., B* **2019**, *243*, 513−521.
(83) Han, D.; Li, B.; Yang, S.; Wang, X.; Gao, W.; Si, Z.; Zuo, Q.; Li, Y.; Li, Y.; Duan, Q.; Wang, D. Engineering charge transfer characteristics in hierarchical Cu_2S QDs@ZnO nanoneedles with p-n heterojunctions: towards highly efficient and recyclable photocatalysts. *Nanomaterials* **2019**, *9*, 16.
(84) Horikoshi, S.; Hidaka, H.; Serpone, N. Environmental remediation by an integrated microwave/UV-illumination method II. Characteristics of a novel UV-VIS-microwave integrated irradiation device in photodegradation processes. *J. Photochem. Photobiol., A* **2002**, *153*, 185−189.
(85) Tachikawa, T.; Ochi, T.; Kobori, Y. Crystal-face-dependent charge dynamics on a $BiVO_4$ photocatalyst revealed by single-particle spectroelectrochemistry. *ACS Catal.* **2016**, *6*, 2250−2256.
(86) Zhang, J. Y.; Xu, J. J.; Tao, F. F. Interface modification of TiO_2 nanotubes by biomass-derived carbon quantum dots for enhanced photocatalytic reduction of CO_2. *ACS Appl. Energy Mater.* **2021**, *4*, 13120−13131.
(87) Kochuveedu, S. T.; Jang, Y. H.; Jang, Y. J.; Kim, D. H. Visible light active photocatalysis on block copolymer induced strings of ZnO nanoparticles doped with carbon. *J. Mater. Chem. A* **2013**, *1*, 898−905.
(88) Cai, T.; Liu, Y.; Wang, L.; Zhang, S.; Zeng, Y.; Yuan, J.; Ma, J.; Dong, W.; Liu, C.; Luo, S. Silver phosphate-based Z-Scheme photocatalytic system with superior sunlight photocatalytic activities and anti-photocorrosion performance. *Appl. Catal., B* **2017**, *208*, 1−13.

https://doi.org/10.1021/acsomega.2c07591
ACS Omega 2023, 8, 7845−7857